ACS Catalysis

Research Article

pubs.acs.org/acscatalysis

Cu−Pt Nanocage with 3-D Electrocatalytic Surface as an Efficient Oxygen Reduction Electrocatalyst for a Primary Zn−Air Battery

Vishal M. Dhavale[†,‡] and Sreekumar Kurungot*[,†,‡]

[†]Physical and Materials Chemistry Division, CSIR-National Chemical Laboratory, Pune 411008, Maharashtra, India

[‡]Academy of Scientific and Innovative Research (AcSIR), Anusandhan Bhawan, 2 Rafi Marg, New Delhi 110001, India

Supporting Information

ABSTRACT: Cu−Pt nanocage (CuPt-NC) intermetallic structures have been prepared by an in situ galvanic displacement reaction. The structures are found to be well organized within the framework demarcated with distinguishing arms, having clear edges and corners with a size of ∼20 nm. The unique nanocage structure possessing large specific surface area and better structural integrity helps to achieve improved electrochemical oxygen reduction reaction activity and stability in alkaline solution in comparison to the commercially available 20 wt % Pt/C. CuPt-NC shows 50 mV positive onset potential shift with significantly higher limiting current in comparison to Pt/C. Interestingly, CuPt-NC has shown 2.9- and 2.5-fold improved mass activity and specific activity, respectively, for ORR at 0.9 V vs RHE in comparison to Pt/C. Moreover, the stability of CuPt-NC has been tested by an accelerated durability test under alkaline conditions. CuPt-NC has been subsequently utilized as the air electrode in a primary Zn−air battery and is found to possess 1.30- and 1.34-fold improved power density and current density at 1 V, respectively, in comparison to the state-of-the-art Pt/C catalyst. In addition, CuPt-NC has shown several hours of constant discharge stability at 20 mA cm^{-2} with a specific capacity of 560 mAh g_{Zn}^{-1} and energy density of 728 Wh kg_{Zn}^{-1} in the primary Zn−air battery system.

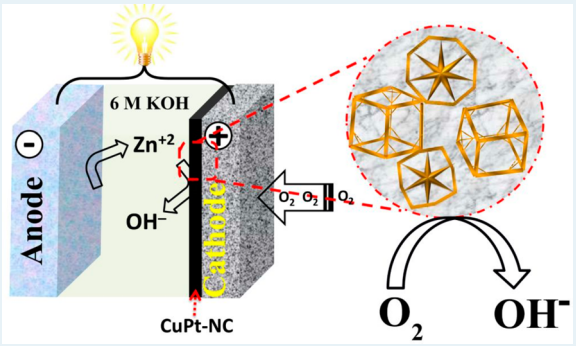

KEYWORDS: *Cu−Pt nanocage, electrocatalyst, oxygen reduction reaction, Zn−air battery, galvanic displacement, 3-D electrocatalytic surface, solvothermal method*

INTRODUCTION

The development of metal−air batteries has attracted substantial research attention due to their applications in portable devices such as hearing aids, toy cars, flashlights, clocks, etc.[1] Among the available metal (M)−air batteries (M = Cd, Zn, Li, Al, etc.), the Zn−air battery is being widely examined due to the low cost, abundance, and environmental benignity of Zn.[1] The Zn−air battery also enjoys high theoretical energy density and long shelf life in comparison to the traditional aqueous batteries.[2,3] However, this prospect is limited by poor performance of the air electrode due to its sluggish oxygen reduction reaction (ORR) activity at the cathode, in comparison to the anodic oxidation of the Zn metal.[1−5] Hence, the development of an efficient cathode catalyst for the Zn−air battery is an existing challenge for the scientific community.[1−5] Hitherto, alloys and core−shell structures of Pt-based metals in the supported form are found to be showing better activity for ORR.[6] Moreover, the limited-localized electronic interaction with the support or within the particles leads to support corrosion, which eventually leads to particle agglomeration during the actual operating conditions.[6] Along with this, the reactant distribution and its utilization are the added issues associated with these types of conventional materials.[6] Additionally, the tedious synthesis protocols involved in the synthesis of the nanostructured electrocatalysts significantly impede the prospects toward the widespread applications of many of these materials in the metal−air batteries.

Recently, researchers started thinking along a different angle by constructing Pt-based materials possessing definite geometrical configuration and composition in order to get better activity with higher utilization.[7,8] Moreover, these nonzero-dimensional structures make the intermetallic nanocage structures less susceptible to dissolution and aggregation during the actual operating conditions in comparison to the available carbon-supported catalysts.[9−11] Consequently, deploying alloys possessing porous nanocage structures could be an elegant solution to effectively tackle the issues related to activity and utilization.[11,12] Recently, Yang, Stamenkovic, et al.[13] have reported the synthesis of Pt−Ni nanoframes by employing a chemical reduction of metal precursors followed by controlled thermal treatment. The formed Pt−Ni nanoframe structure has shown 36- and 22-fold enhanced mass and specific activity, respectively. Similarly, recently, many more researchers have

Received: October 13, 2014
Revised: January 21, 2015
Published: January 21, 2015

DOI: 10.1021/cs501571e
ACS Catal. 2015, 5, 1445−1452

Scheme 1. Schematic Representation of a Primary Zn−Air Battery with CuPt-NC as the Cathode

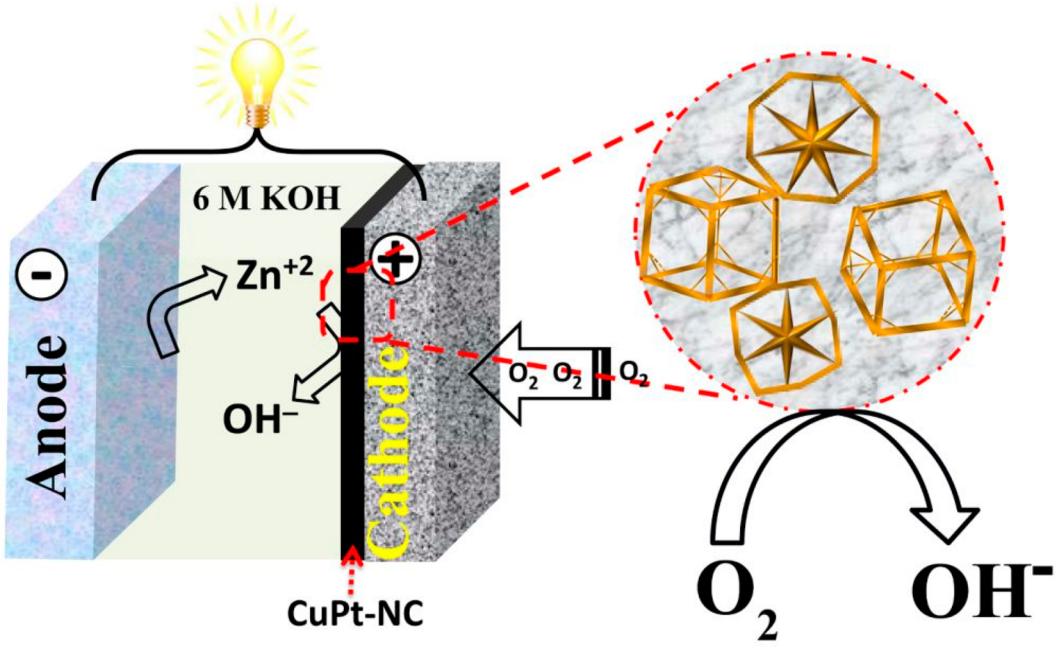

been involved in the synthesis of nonzero cage structures on the basis of the Kirkendall effect and galvanic displacement method and explored such materials for the application of ORR.[13−15] Many multimetallic nanocage structures have shown improved performance and stability in fuel cell applications.[11,16−18] This property modulation is credited to the possible electronic changes, systematic atomic arrangement, presence of more voids and edges, higher surface-to-volume ratio, more accessible active sites, etc.[9−15]

In most cases, the adopted synthetic protocols such as template-assisted methods (hard, soft, sacrificial templates), chemical reduction methods, etc. are very tedious and time demanding.[11,18] At the same time, the interruption and surface passivation of the metal by the organic and/or inorganic structure directing agents make the chemistry very difficult in achieving the desired product with definite geometry.[11,17,18] In parallel, during bulk synthesis, controlling simultaneously the growth, size, and geometry of the crystal is a tricky job. Therefore, achieving high and consistent energy and power densities with these types of intermetallic electrocatalysts is a very difficult task. Most of the nanocage structures have been prepared with low energy density materials (such as Co-oxide, Mn-oxide, Mg-oxide, etc.).[11,17] Hence, there is less structural stability under actual operating conditions. Therefore, a key solution is to develop novel ORR electrocatalysts with high energy density materials (such as Cu−Pt, Pd−Pt, Fe−Pt, etc.) which could fulfill the requirement of efficient ORR activity along with higher energy output in the Zn−air battery. Traditional batteries normally follow a complicated intercalation−deintercalation mechanism during the charge−discharge process, which limits the actual achievable energy density by the systems. In this perspective, substitution of the intercalation material (cathode electrode) with a catalytically active ORR electrode may solve the existing energy density issue of the traditional storage devices.[1−3] In this context, metal−air batteries (mainly Zn−air) can be a very good option and can attain a very high energy density of 1100 Wh kg^{-1}, possibly due to the absence of the intercalation process.[1−3] Herein, we demonstrate that utilization of a nanocage catalyst based on Cu and Pt (CuPt-NC) can serve as a potential cathode material for a Zn−air battery (Scheme 1) with enhanced activity and durability characteristics. Recently, Lou et al. have synthesized a Cu−Pt nanocage structure, which was investigated toward methanol oxidation.[17] The applications of such materials so far have been mainly restricted to methanol oxidation.[7,17,19] However, we observed that these types of systems possess great potential to tackle the sluggish electrode kinetics in metal−air batteries. Consequently, it is worthwhile to explore their unique structural characteristics in electrocatalysis. Herein, we report how a primary Zn−air battery fabricated by using CuPt-NC structures as the cathode could outperform the cathode derived from the state-of-the-art Pt/C catalyst. CuPt-NC was prepared by in situ galvanic displacement reaction between Cu particles and Pt ions by solvothermal methods.[17] Here, the peculiar morphology, 3-D electrocatalytic surface, and higher surface active area of CuPt-NC help the system to provide high ORR activity in alkaline medium, which eventually could be utilized in the battery system by deploying the material as the cathode catalyst. In the present work, we have specifically tried to find out the activity modulation accomplished in the system by considering the structural advantages such as the 3-D morphology, which leads to high surface area, accessible active sites, and modulated property characteristics of the active centers.

EXPERIMENTAL SECTION

Materials. Chloroplatinic acid ($H_2PtCl_6·6H_2O$), copper(II) acetylacetonate (Cu $(acac)_2$), oleylamine, and cetyltrimethylammonium bromide (CTAB) were procured from Sigma-Aldrich, and toluene and ethanol were purchased from Thomas Baker. The chemicals were used as such without any further purification. Zn powder was purchased from J K Impex.

Synthesis of Cu−Pt Intermetallic Nanocage (CuPt-NC) Structures. The Cu−Pt intermetallic nanocage structures have been prepared by following the reported procedure.[17] Briefly, 8 wt % of chloroplatinic acid solution was prepared in 200 mg of

DOI: 10.1021/cs501571e
ACS Catal. 2015, 5, 1445−1452

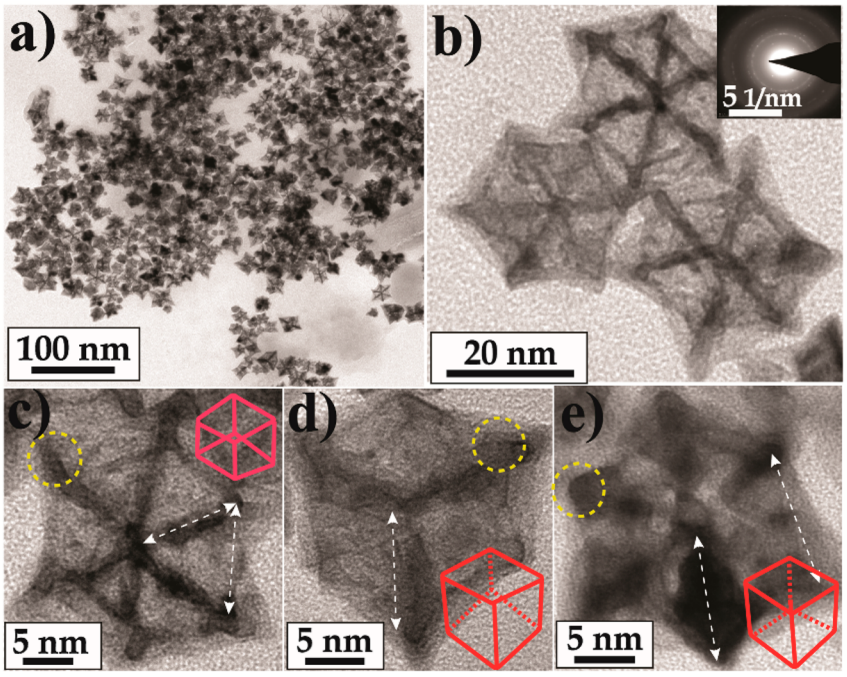

Figure 1. TEM images of (a) the CuPt-NC intermetallic nanocage structures indicating the good dispersion of CuPt-NC in solution, (b) HR-TEM images of CuPt-NC (inset SAED pattern), and (c–e) the hexagonal, cubical, and pentagonal structures of CuPt-NC with their representative model structure frameworks (inset), respectively.

oleylamine, and 20 mg of copper acetylacetonate was dispersed in 8 mL of fresh oleylamine by sonicating it in a Branson water bath sonicator. Subsequently, 50 mg of CTAB was added and the sonication was extended for a further 30 min. The well-dispersed solution was transferred into a 15 mL Teflon-coated stainless steel autoclave and was subjected to heating at 180 °C for 24 h. Finally, the reaction mixture was centrifuged at 10000 rpm and washed with a toluene/ethanol (3/2) mixture and the material was dried at 60 °C in an oven. The material collected after this stage was used as such for further characterization.

Structural Characterization. For high-resolution transmission electron microscope (HR-TEM) analysis, a well-dispersed catalyst solution was prepared by sonicating 1 mg of the catalyst in 5 mL of isopropyl alcohol. This catalyst-dispersed solution was drop-coated on a carbon-coated (200 mesh) Cu grid. The sample-coated grid was dried under a lamp for 5 h, and the images were obtained on an FEI TECNAI G2 F20 instrument. The operation conditions are accelerated voltage 200 kV, C_s = 0.6 mm, and resolution 1.7 Å. The crystallinity of the catalyst was determined by recording X-ray diffraction (XRD) patterns on a PANalytical instrument under the conditions of wavelength (λ) 1.54 Å (Cu Kα radiation), scanning rate 2° min^{-1}, and step size 0.02° in 2θ. X-ray photoelectron spectroscopy (XPS) measurements were carried out on a VG Micro Tech ESCA 300° instrument at a pressure of >1 × 10^{-9} Torr (pass energy 50 eV, electron takeoff angle 60°, and overall resolution ~0.1 eV).

Electrochemical Studies. A Bio-Logic (VMP-3) instrument was used to investigate the electrochemical properties by cyclic voltammetry (CV) and rotating-disk-electrode (RDE) (Pine Instruments) studies in a conventional three-electrode test cell with Hg/HgO as the reference electrode and platinum foil as the counter electrode. Moreover, the potential value was normalized with respect to the reversible hydrogen electrode (RHE). Prior to the start of the electrochemical study, the working electrode (glassy-carbon RDE) was polished with 0.3 μm alumina slurry and was sonicated for a few minutes in acetone and then in DI water. The catalyst slurry was prepared by sonicating 5 mg of the electrocatalyst in 1 mL of a 3/2 ethanol/DI water mixture, and subsequently this was drop-coated on a previously polished glassy-carbon RDE. Moreover, the coating was maintained to achieve a constant Pt loading of 10 μg, and then 5 μL of a 0.01 wt % Fumion solution (used as a binder) was applied on the whole surface of the disk electrode to yield a uniform thin film. Subsequently, the electrode was dried under an IR lamp and was used as the working electrode for the electrochemical investigations. An aqueous solution of 0.1 M KOH, deaerated with N_2 gas, was used as an electrolyte for the CV and RDE studies. Moreover, the measured current was divided by the geometrical area of the glassy-carbon RDE (0.19625 cm^2).

Primary Zn–Air Battery Testing. To construct the Zn–air battery, the air electrode was prepared by coating a dispersed solution of CuPt-NC in isopropyl alcohol onto the porous carbon paper (1 cm^2) to achieve 2 mg_{Pt} cm^{-2} loading and paired with Zn powder coated porous carbon paper (anode electrode) in 6 M KOH, which acts as the electrolyte. The battery testing was performed at room temperature, and the electrolyte was continuously purged with oxygen (0.2 standard L min^{-1}). The system showed an initial open circuit voltage of 1.3–1.4 V. Moreover, the voltage stability of the Zn–air battery cell was tested at different discharge rates: viz., 20, 25, 30, and 35 mA cm^{-2}. The results obtained with CuPt-NC were compared with a system made by using commercially available 20 wt % Pt/C at the cathode, having similar loading. Similarly, the steady-state polarization was measured with the same setup under the continuous purging of oxygen at a potential scan rate of 5 mV s^{-1}.[3] The electrodes were prepared by brush coating, shown in Scheme S1 in the Supporting Information.

DOI: 10.1021/cs501571e
ACS Catal. 2015, 5, 1445–1452

RESULTS AND DISCUSSION

Figure 1a displays homogeneous and well-dispersed distribution of the nanoparticles of CuPt-NC in solution. High-resolution TEM (HR-TEM) images of CuPt-NC are given in Figure 1b,c. The structures are found to be well organized within the framework demarcated with distinguishing arms having clear edges and corners (shown in Figure 1c−e with white two-sided arrows and yellow circles). The HR-TEM images clearly indicate the formation of cubical, pentagonal, and hexagonal structures (Figure 1c−e) with an average size of ∼20 nm. A close inspection of the TEM images (Figure 1c−e) reveals that these nanocages have an observable hollow structure (the model structures are shown in the insets of Figure 1c−e). Some of the particles, however, seem to be like hexagonal stars because of their particular orientation. Moreover, the crystallinity of CuPt-NC is confirmed through a selected area electron diffraction (SAED) pattern (Figure 1b, inset). It has been documented that this kind of morphology will be formed due to the complex chemistry between the metal precursors and the surfactant and/or the reducing agent used via the nanoengineering process. The nanoengineering of CuPt-NC is mainly associated with the chemistry involved during the synthesis (a detailed explanation is given in the Supporting Information).[11,17]

Comparative X-ray diffraction patterns of CuPt-NC and Pt/C are given in Figure 2. The well-distinguished peaks at 2θ = 39.9, 46.5, and 68.8° correspond to the (111), (200), and (220) planes of the fcc crystal of Pt. Moreover, the clear difference in the diffraction peak of CuPt-NC in comparison to Pt/C validates the decrease in the *d*-spacing value (marked with the black dotted line in Figure 2).[17] However, in comparison with the literature reports, it seems that the (111/200) ratio is lower in the case of the alloys (1.24) in comparison to CuPt-NC (2.01).[17,20] The shift in the peaks certifies the lattice contraction, which is attributed to the change in electronic structure as well as the geometrical nature of the Cu−Pt structure, which ultimately decreases the interatomic distance of the Pt atoms.[19−21]

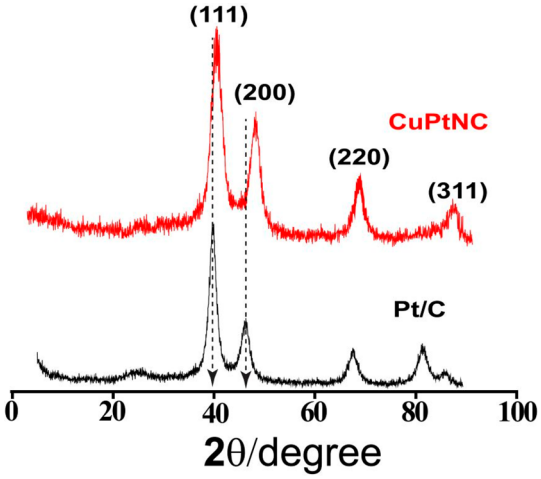

Figure 2. Comparative X-ray diffraction patterns of 20 wt % Pt/C and CuPt-NC.

The mutual interaction between Cu and Pt in the intermetallic structure and change in the electronic environment has also been confirmed through X-ray photoelectron spectroscopic (XPS) investigation (Figure 3 and Figure S2 in the Supporting Information). The full survey scan of CuPt-NC has shown in Figure S2a. The presence of Cu, Pt, and O is marked in the figure. Subsequently, the deconvoluted XPS of Cu shown in Figure 3a, which gives two peaks at 933.08 and 953.20 eV, which are assigned to Cu $2p_{3/2}$ and $2p_{1/2}$, respectively. Moreover, the characteristic satellite peaks are observed at ∼942 and ∼962 eV of Cu $2p_{3/2}$ and $2p_{1/2}$, respectively. The satellite peaks also can be deconvoluted, which show the presence of two subpeaks, attributed to the Cu present in two different oxidation states.[16] Moreover, XPS of Pt shows the presence of four peaks originating from the spin−orbit splitting of Pt $4f_{7/2}$ and $4f_{5/2}$ (Figure 3b). The peaks at binding energies of ∼71.6 (Pt $4f_{7/2}$) and 74.9 eV (Pt $4f_{5/2}$) are attributed to the Pt^0 state and the peaks at 72.8 and 76.5 eV are assigned to the Pt^{+x} state of the CuPt-NC structures. However, in the case of Pt/C, the $4f_{7/2}$ and $4f_{5/2}$ peaks appear at slightly lower binding energy: i.e., 71.2 and 74.4 eV (Figure S4). The relatively high intensity of Pt^0 with respect to that of Pt^{+x} shows that the Pt in both the catalysts is principally metallic in nature. Moreover, the shift in the binding energy of Pt peaks for CuPt-NC indicates the effective charge transfer between Cu and Pt, possibly due to the change in the electronic structure of Pt in the case of CuPt-NC.[17,21] XPS profiles of Pt 4f, C 1s, and O 1s of 20 wt % Pt/C are shown in Figure S4 in the Supporting Information. Moreover, the relative composition of the Cu to Pt in CuPt-NC has been calculated from the XPS data and is found to be 1:1.023. Subsequently, the Cu:Pt stoichiometry is

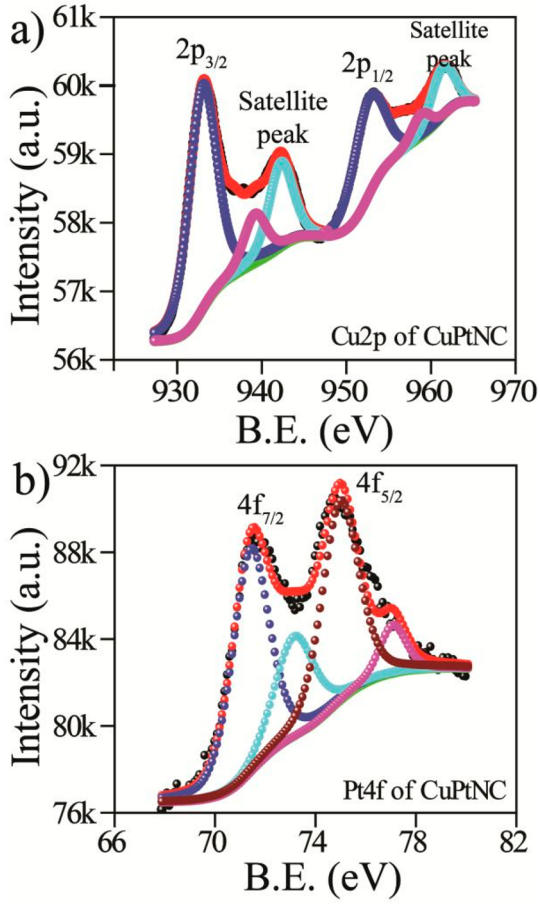

Figure 3. Deconvoluted XPS: (a) Cu 2p of CuPt-NC; (b) Pt 4f of CuPt-NC.

DOI: 10.1021/cs501571e
ACS Catal. 2015, 5, 1445−1452

found to be 3:1 in CuPt-NC (detailed explanation is given in the Supporting Information).

The formed nanocage structures possess a beautiful open-faceted hollow geometry with ordered atomic arrangement within the structure. As already shown in Figure 1, CuPt-NCs are formed by interconnected arms of CuPt which are arranged into a 3-D network. To get a clear and easy understanding of the formed structures, the model structures are also shown in the insets of Figure 1c–e. It seems that the formed CuPt-NCs are hollow structures possessing open facets in all directions. In addition, these open facets increase the overall active sites and provide easy molecular accessibility within the structure. In view of this, we termed this open 3-D structure having facile molecular accessibility as a 3-D electrocatalytic surface.[13,17]

Furthermore, to investigate the electrochemical activity of CuPt-NC, we have carried out cyclic voltammetry (CV) analysis and linear sweep voltammetry (LSV) (Figure S6 in the Supporting Information). Moreover, for comparison, we have done similar investigation with commercial 20 wt % Pt/C (Figure S5 in the Supporting Information). Figure 4

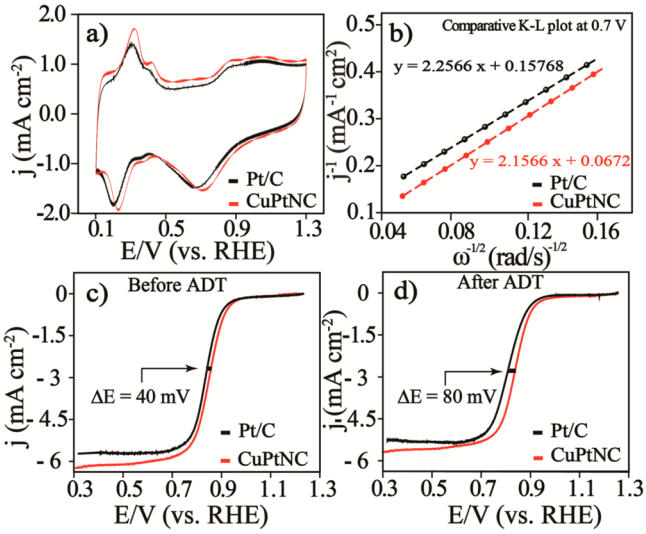

Figure 4. Comparative electrochemical data of CuPt-NC with 20 wt % Pt/C: (a) CV recorded in N_2-saturated 0.1 M KOH at 50 mV s^{-1}; (b) K-L plots of Pt/C and CuPt-NC made at 0.7 V (vs RHE); (c, d) LSVs taken before and after ADT, recorded in O_2-saturated 0.1 M KOH with a scan rate of 10 mV s^{-1} at 1600 rpm.

summarizes the comparative electrochemical results of CuPt-NC with 20 wt % Pt/C performed in 0.1 M KOH. The comparative CV of CuPt-NC and Pt/C is presented in Figure 4a. The CV features are similar to those of the polycrystalline Pt electrode.[17] In both CVs, the hydrogen adsorption–desorption and oxygen reduction peaks appear in the potential ranges 0.1–0.4 V, and 0.6– 1 V (vs RHE), respectively. The peak integral of the hydrogen desorption region gives charge values equal to 1.43 and 1.23 mC for CuPt-NC and Pt/C, respectively. The obtained ECSA and roughness factor (RF) for CuPt-NC are 68 m^2 g_{Pt}^{-1} and 34.65, respectively, whereas the corresponding values for Pt/C are 58.57 m^2 g_{Pt}^{-1} and 29.85, respectively (details of the calculations are provided in the Supporting Information). The slight increment in ECSA for the former could be assigned to the higher number of accessible Pt active sites of CuPt-NC in comparison to Pt/C. CV results show that CuPt-NC has a positive onset potential shift as well as a higher peak current density for oxygen reduction in comparison to Pt/C (Figure 4a).

In addition, a hydrodynamic voltammogram for the ORR using RDE techniques has been recorded by varying the rotation speed of the working electrode from 400 to 2500 rpm (Figures S5b and S6b in the Supporting Information). It has been observed that the current increases with an in increase in the rotation speed of the working electrode, which clearly reveals the facile mass transport of oxygen to the electrode surface (details about the RDE and related equations are given in the Supporting Information). Moreover, the exact mechanism of the ORR has been confirmed through the Koutecky–Levich (K-L) analysis and the obtained K-L plots are shown in Figures S5d and S6d in the Supporting Information. The K-L plots show good linearity, which is assigned to the first-order kinetics of ORR, and both catalysts are found to follow similar mechanistic pathways.[22] The number of electrons (n) transferred during the reaction has been obtained from the slope of the K-L plot, which is found to be ~4 (Figure 4b). Moreover, the reciprocal of the intercept of the K-L plot provides the kinetic current (Figure 4b). It has been observed that CuPt-NC (1.49×10^{-3} mA) has shown kinetic current improved by 1 order of magnitude in comparison to Pt/C (6.34×10^{-4} mA), which highlights the structural benefit of the nanocage over the spherical particles toward the ORR. Further into the mechanism of ORR and quality of the electrocatalyst can be obtained from Tafel analysis and mass and specific activity comparisons. In view of this, comparative mass transport corrected Tafel plots, which is a graph of E vs log $|j_k|$, are given in Figure S7 in the Supporting Information. The Tafel slopes of Pt/C and CuPt-NC are found to be ~77.40 and ~69.94 mV $decade^{-1}$, respectively. It should be noted that the Tafel slope provides an indication of the actual mechanism taking place on the electrode surface and is related to the state of the adsorbed oxygen species and its coverage variation with respect to the potential. The lower Tafel slope obtained in the case of CuPt-NC stands out as an important indicator of its improved performance, which originates from the facile oxygen adsorption and the subsequent reduction processes on the nanocage surface.[21] Details about the calculation of mass-corrected kinetic current are given in the Supporting Information. We have also calculated the mass and specific activity of Pt/C and CuPt-NC at 0.9 V (vs RHE), as shown in Figure S8 in the Supporting Information. CuPt-NC exhibits a mass activity of 0.32 A mg_{Pt}^{-1}, which is 2.9-fold higher than that of the Pt/C catalyst (0.11A mg_{Pt}^{-1}) at 0.9 V (vs RHE). Moreover, CuPt-NC displays a specific activity (calculated at 0.9 V (vs RHE)) of 0.47 mA cm^{-2}, which is 2.5-fold higher in comparison to Pt/C (0.19 mA cm^{-2}) (Figure S8). This improved mass activity and specific activity of CuPt-NC over Pt/C is mainly credited to the well-defined atomic arrangement, overall structural integrity, and higher number of active centers of the open-faceted nanocage framework (details on the mass activity and specific activity calculation are given in the Supporting Information).

To fulfill the desire for the effective utilization of CuPt-NC in realistic applications, stability in an electrochemical environment is an obligatory requirement. Therefore, the ADT has been performed by potential cycling (1000 cycles) in a potential window of 0.5–1.3 V (vs. RHE), with a voltage scan rate of 50 mV s^{-1} in oxygen-saturated 0.1 M KOH solution, at room temperature. LSV has been recorded before and after ADT to investigate the performance degradation.

DOI: 10.1021/cs501571e
ACS Catal. 2015, 5, 1445–1452

Table 1. Summary of the Electrochemical Analysis

	before ADT			after ADT					
sample name	onset potential (V)	$E_{1/2}$ (V)	limiting current (mA cm^{-2})	onset potential (V)	$E_{1/2}$ (V)	limiting current (mA cm^{-2})	decrease in limiting current (%)	$\Delta E_{1/2}$ (V)	I_k @ 0.7 V (mA)
Pt/C	0.90	0.806	5.75	0.9	0.728	5.0	13	0.078	6.34×10^{-4}
CuPt-NC	0.95	0.846	6.25	0.95	0.816	6.0	4	0.030	1.49×10^{-3}

Figure 4c,d shows the comparative LSVs of CuPt-NC and Pt/C, before and after ADT, respectively. After 1000 cycles, the half-wave potential ($E_{1/2}$) is decreased by 78 and 30 mV for Pt/C and CuPt-NC, respectively (Figures S5c and S6c in the Supporting Information, Table 1). Moreover, the limiting current is also found to be better for CuPt-NC in comparison to that of Pt/C (Figures S5c and S6c and Table 1). Moreover, CuPt-NC (onset potential is 0.95 V) has shown a 50 mV positive onset potential shift in comparison to Pt/C (onset potential is 0.90 V) (Figure 4c,d and Table 1). Furthermore, the difference in $E_{1/2}$ between the CuPt-NC and Pt/C systems is found to be 40 and 80 mV before and after ADT (Figure 4c,d). The observed higher limiting current for CuPt-NC in comparison to that of Pt/C could be attributed to the improved diffusion of oxygen and, subsequently, to its better interaction with the active sites located in CuPt-NC. Furthermore, both catalysts follow the direct reduction mechanism of ORR involving the four-electron transfer, which produces OH^- (Figures S5d and S6d). The better productivity of CuPt-NC is mainly attributed to its structure, which ultimately provides a higher number of the catalytically active sites, easily accessible space, synergetic effect of Cu and Pt, etc. The sites are more favorable for the dissociative adsorption of oxygen during ORR in alkaline medium.

Furthermore, to understand the exact cause behind the decrease in the limiting current and change in half-wave potential value, we have done the comparative compositional analysis of CuPt/NC by an XPS study,[23] before (Figure 3 and Figure S2 in the Supporting Information) and after (Figure S3 in the Supporting Information) ADT. CuPt-NC has shown 46.44, 47.52, and 6.06 wt % of Cu, Pt, and O, respectively, before ADT. After ADT, the amounts corresponding to Cu, Pt, and O are found to be 46.14, 47.22, and 6.64 wt %, respectively. A close analysis of the XPS data reveals that the relative composition of the metals (i.e., Cu:Pt) is the nearly same (1:1.023) and the stoichiometric ratio is also found to be the same (Cu:Pt is 3:1) before and after ADT. However, more interestingly, the amount of O is found to be slightly increased from 6.06 to 6.64 wt %. This indicates higher oxidation of the surface metal atoms during ADT without affecting their relative metal composition (Cu:Pt = 1:1.023) and stoichiometry (Cu_3Pt). In other words, the obtained results stand out as a proof for the structural integrity of the intermetallic hollow CuPt-NC structure. The increased oxygen weight percent at the surface might be a reason for the decrease in the half-wave potential and limiting current of CuPt-NC after 1000 cycles of ADT because the increased O weight percent might be due to the higher oxidation of the active metal centers. On the other hand, in the case of Pt/C, the main reason for the decrease in the limiting current is attributed to the higher oxidation of the carbon support under the potential cycling in a window of 0.5−1.3 V (vs RHE). The oxidation of the support may leave naked Pt nanoparticles, which results in aggregation of the particles, leading to a decrease in the surface-to-volume ratio and thereby the overall activity. Hence, the aggregation of Pt particles in the case of Pt/C and higher oxidation of active metal centers in the case of CuPt-NC could be the reasons for the decrease in the limiting current.

The superior ORR activity of CuPt-NC as evident from the RDE study, however, is not sufficient to conclude that the system can ensure an enhanced performance in a practical Zn−air battery, because the concentration of the dissolved oxygen will be different in the electrolyte used for the LSV investigation (0.1 M KOH) and the electrolyte used in the battery testing (6 M KOH). Along with this, the overall performance will also be decided by the formation of an effective triple-phase boundary, which could be effectively tackled in the case of a nanocage structure. Hence, it is necessary to analyze the material under similar electrolyte conditions which are favorable for the Zn−air battery.

The fabricated Zn−air battery is composed of CuPt-NC as the air electrode material (cathode), Zn powder as the anode material, and 6 M KOH as the electrolyte (Scheme 1). Instead of using Ni foil or any other kind of oxygen evolution (OER) materials, we coated the CuPt-NC catalyst on a polytetrafluoroethylene (PTFE) treated carbon paper (active area 1 cm^2), which avoids additional intrinsic electrochemical activity interference within the system. In principle, Zn undergoes oxidation at the anode and oxygen gets reduced at the cathode. The actual reaction mechanism is shown in the Supporting Information. Here, we have compared the performance of the CuPt-NC coated electrodes for ORR in the primary Zn−air battery with that of the commercially available Pt/C. The cathode Pt loading was kept as 2 mg cm^{-2} in both systems. The detailed electrode fabrication is given in the Experimental Section. The Zn powder and CuPt-NC coated carbon papers were dipped in 6 M KOH solution, and oxygen was purged at the cathode side. The separately fabricated Zn−air battery setups with CuPt-NC and Pt/C as the air electrodes have shown open circuit potentials of ∼1.4 and ∼1.3 V (Figure 5a and Figure S9 in the Supporting Information), respectively. The improved open circuit potential in the case of the system having CuPt-NC as the cathode is attributed to the higher number of active centers and ECSA possessed by CuPt-NC, which has already been confirmed through cyclic voltammetric investigations. The comparative steady-state polarization curves of CuPt-NC and Pt/C as the cathodes are shown in Figure 6. The CuPt-NC based device shows a current density of 253.8 mA cm^{-2}, whereas the device based on Pt/C gives a current density of 188.8 mA cm^{-2} at a voltage of 1 V (Figure 6). Moreover, the peak power density is found to be 1.3-fold higher for the CuPt-NC as an air electrode in comparison to Pt/C (Figure 6). The improved current density at 1 V and the peak power density of the device fabricated with CuPt-NC as the air electrode is mainly attributed to the higher ORR activity of CuPt-NC over Pt/C. In addition, to investigate the robustness of the primary Zn−air batteries made with CuPt-NC over those made with Pt/C, the system was subjected to galvanostatic discharge and the polarization curve was recorded at different discharge current rates ranging from 20 to 35 mA cm^{-2}. No

DOI: 10.1021/cs501571e
ACS Catal. 2015, 5, 1445−1452

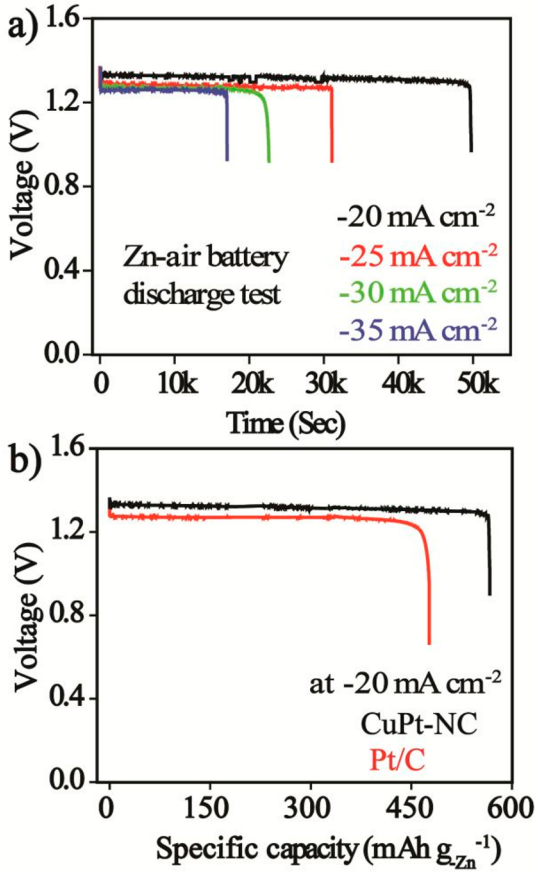

Figure 5. (a) Discharge curves of a primary Zn−air battery performed with different discharge current densities (20−35 mA cm^{-2}) until the complete consumption of Zn. (b) Comparative specific capacity vs potential plot of CuPt-NC and 20 wt % Pt/C at a discharge current density of 20 mA cm^{-2}. The plots in Figure 5b are created from the data of Figure 5a and Figure S9 in the Supporting Information, by normalizing the values with the amount of Zn consumed (∼0.5 g). Conditions: anode, Zn powder coated carbon paper; cathode, CuPt-NC or Pt/C coated carbon paper (2 mg_{Pt} cm^{-2}); electrolyte, 6 M KOH; active area, 1 cm^2.

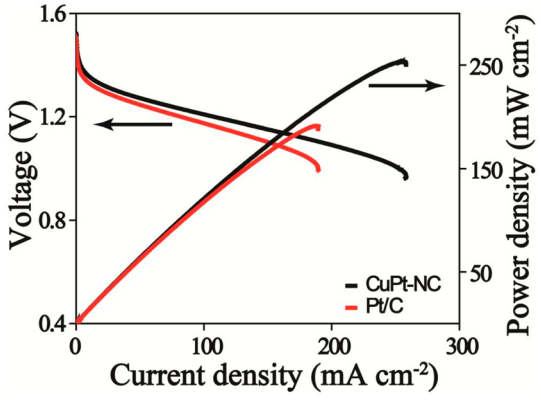

Figure 6. Comparative steady-state polarization curves (*I*−*V*) and corresponding power density plots of the batteries fabricated by using CuPt-NC and Pt/C as the cathode catalysts. Conditions: anode, Zn powder coated carbon paper; cathode, Pt/C or CuPt-NC coated carbon paper (2 mg_{Pt} cm^{-2}); electrolyte, 6 M KOH; active area, 1 cm^2.

abrupt potential drop is observed for a long time, showing the absence of any catastrophic failure of the integrated assembly with CuPt-NC as the cathode (Figure 5a). The higher discharge stability obtained for CuPt-NC (∼14 h, Figure 5a) in comparison to Pt/C (∼12 h, Figure S9), at a discharge rate of 20 mA cm^{-2}, is attributed to the higher ORR activity of CuPt-NC in the battery and its inherent structural integrity. As the galvanostatic discharge continues, the Zn undergoes oxidation, becoming thinner and thinner. Ultimately, the electrolyte accumulates more and more Zn salts and the battery eventually stops functioning once all of the Zn metal is consumed (Figure 5a and Figure S9). In addition, the specific capacity is found to be better for CuPt-NC in comparison to Pt/C (Figure 5b, discharge rate 20 mA cm^{-2}). The specific capacity calculated by normalizing current with the mass of the consumed Zn[5] (∼0.5 g) is 560 and 480 mAh g_{Zn}^{-1} for CuPt-NC and Pt/C, respectively. Correspondingly, CuPt-NC has shown a high energy density of 728 Wh kg_{Zn}^{-1} in comparison to Pt/C (624 Wh kg_{Zn}^{-1}). The superior activity for CuPt-NC is mainly credited to its peculiar structure, which helps the system to effectively maintain active center density and easily accessible space along with the electronic modulations affected in the system, which facilitates effective dissociation of oxygen. Therefore, the obtained system could be developed with many more different metals and could be utilized for many more electrochemical applications such as metal−air batteries, fuel cells, etc.

CONCLUSIONS

CuPt-NC intermetallic nanocage structures have been synthesized by a simple solvothermal method via an in situ galvanic displacement reaction between Cu and Pt, and their enhanced oxygen reduction activity and stability in comparison to those of Pt/C in alkaline solution could be explored. CuPt-NC has shown 2.9- and 2.5-fold improved mass activity and specific activity, respectively, for ORR at 0.9 V vs RHE in comparison to Pt/C. Utilization of CuPt-NC as the air cathode in a primary Zn−air battery delivered 1.30 and 1.34 times improved power density and current density at 1 V, respectively, in comparison to that of the state-of-the-art Pt/C catalyst. Moreover, during the primary Zn−air battery testing, CuPt-NC led to a superior specific capacity and energy density (560 mAh g_{Zn}^{-1} and 728 Wh kg_{Zn}^{-1}, at a discharge rate of 20 mA cm^{-2}), in comparison to the performance of the system possessing Pt/C as the cathode (480 mAh g_{Zn}^{-1} and 624 Wh kg_{Zn}^{-1}, at a discharge rate of 20 mA cm^{-2}). In particular, CuPt-NC, with its high density of surface defects, potentially offers more active site density for facilitating efficient dissociative adsorption of oxygen, resulting in improved ORR activity. The synergetic interaction between Pt and Cu also plays a favorable role in the efficient adsorption and bond polarization of oxygen. The primary Zn−air batteries prepared with CuPt-NC electrocatalyst are found to be very robust, which indicates the survivability of the system under the electrochemical environment conditions.

ASSOCIATED CONTENT

Supporting Information

The following file is available free of charge on the ACS Publications website at DOI: 10.1021/cs501571e.

Schematic representation of the cathode and anode electrodes prepared by coating CuPt-NC and Zn powder on polytetrafluoroethylene (PTFE) treated carbon paper, TEM images of the commercially available 20 wt % Pt/C, XPS full survey scan of CuPt-NC, O 1s spectra of CuPt-

DOI: 10.1021/cs501571e
ACS Catal. 2015, 5, 1445−1452

NC before ADT, XPS of Cu 2p, Pt 4f, and O 1s of CuPt-NC after ADT, XPS of the commercially available 20 wt % Pt/C along with deconvoluted XPS of Pt 4f, C 1s, O 1s spectra, comparative CV, LSV at different rpm, stability test, Tafel plot, K-L plots at different potentials of Pt/C and CuPt-NC, comparative mass and specific activity plots of Pt/C and CuPt-NC, and discharge test (at different current densities) of the primary Zn−air battery for Pt/C as cathode (PDF)

AUTHOR INFORMATION

Corresponding Author

*S.K.: fax, +91-20-25902636/2615; tel, +91-20-25902566; e-mail, k.sreekumar@ncl.res.in.

Notes

The authors declare no competing financial interest.

ACKNOWLEDGMENTS

This study was financially supported by Council of Scientific and Industrial Research (CSIR), New Delhi, India, by project funding (CSC0122) to S.K. and research fellowship to V.M.D. The authors thank Dr. K. R. Patil for the XPS analysis. The authors are grateful to Dr. Sourav Pal, Director of CSIR-National Chemical Laboratory, Pune, India, for providing infrastructure and constant support.

REFERENCES

(1) (a) Linden, D.; Reddy, T. B. *Handbooks of Batteries*; McGraw-Hill: New York, 2002. (b) Chen, Z.; Yu, A.; Higgins, D.; Li, H.; Wang, H.; Chen, Z. *Nano Lett.* **2012**, *12*, 1946−1952.

(2) Lee, J.-S.; Kim, S. T.; Cao, R.; Choi, N.-S.; Liu, M.; Lee, K. T.; Chao, J. *Adv. Energy Mater.* **2011**, *1*, 34−50.

(3) Li, Y.; Gong, M.; Liang, Y.; Feng, J.; Kim, J.-E.; Wang, H.; Hong, G.; Zhang, B.; Dai, H. *Nat. Commun.* **2013**, *4*, 1805.

(4) Girishkumar, G.; McCloskey, B.; Luntz, A. C.; Swanson, S.; Wilcke, W. *J. Phys. Chem. Lett.* **2010**, *1*, 2193−2203.

(5) Scrosati, B.; Hassoun, J.; Sun, Y.-K. *Energy Environ. Sci.* **2011**, *4*, 3287−3295.

(6) (a) Lim, B.; Yu, T.; Xia, Y. *Angew. Chem., Int. Ed.* **2010**, *49*, 9819−9820. (b) Xu, D.; Liu, Z. P.; Yang, H. Z.; Liu, Q. S.; Zhang, J.; Fang, J. Y.; Zou, S. Z.; Sun, K. *Angew. Chem., Int. Ed.* **2009**, *48*, 4217−4221. (c) Strasser, P.; Koh, S.; Anniyev, T.; Greeley, J.; More, K.; Yu, C.; Liu, Z.; Kaya, S.; Nordlund, D.; Ogasawara, H.; Toney, M. F.; Nilson, A. *Nat. Chem.* **2010**, *2*, 454−460. (d) Sau, T. K.; Rogach, A. L.; Jackel, F.; Klar, T. A.; Feldmann, J. *Adv. Mater.* **2010**, *22*, 1805−1825. (e) Snyder, J.; Fujita, T.; Chen, M. W.; Erlebacher, J. *Nat. Mater.* **2010**, *9*, 904−907. (f) Barbir, F. *PEM Fuel Cells: Theory and Practice*, 2nd ed.; Elsevier: San Diego, CA, 2005. (g) Carrette, L.; Friedrich, K. A.; Stimming, U. *Fuel Cells* **2001**, *1*, 5−39.

(7) (a) Chen, Z. W.; Waje, M.; Li, W. Z.; Yan, Y. S. *Angew. Chem., Int. Ed.* **2007**, *46*, 4060−4063. (b) Alia, S. M.; Zhang, G.; Kisailus, D.; Li, D. S.; Gu, S.; Jensen, K.; Yan, Y. S. *Adv. Funct. Mater.* **2010**, *20*, 3742−3746. (c) Wang, R.; Xu, C.; Bi, X.; Ding, Y. *Energy Environ. Sci.* **2012**, *5*, 5281−5286.

(8) (a) Sasaki, K.; Wang, J. X.; Naohara, H.; Marinkovic, N.; More, K.; Inada, H.; Adzic, R. R. *Electrochim. Acta* **2010**, *55*, 2645−2652. (b) Long, N. V.; Yang, Y.; Thi, C. M.; Minh, N. V.; Cao, Y.; Nogami, M. *Nanoenergy* **2013**, *2*, 636−676. (c) Favilla, P. C.; Acosta, J. J.; Schvezov, C. E.; Sercovich, D. J.; Collet-Lacoste, J. R. *Chem. Eng. Sci.* **2013**, *101*, 27−34. (d) Zhou, X.; Gan, Y.; Du, J.; Tian, D.; Zhang, R.; Yang, C.; Dai, Z. *J. Power Sources.* **2013**, *232*, 310−322. (e) Zhang, G.; Shao, Z.-G.; Lu, W.; Xie, F.; Qin, X.; Yi, B. *Electrochim. Acta* **2013**, *103*, 66−76.

(9) (a) Hong, J. W.; Kang, S. W.; Choi, B. S.; Kim, D.; Lee, S. B.; Han, S. W. *ACS Nano* **2012**, *6*, 2410−2419. (b) Feng, Y.-Y.; Zhang, G.-R.; Ma, J.-H.; Liu, G.; Xu, B.-Q. *Phys. Chem. Chem. Phys.* **2011**, *13*, 3863−3872. (c) Snyder, J.; McCue, I.; Livi, K.; Erlebacher, J. *J. Am. Chem. Soc.* **2012**, *134*, 8633−8645.

(10) (a) Mahmoud, M. A.; Qian, W.; El-Sayed, M. A. *Nano Lett.* **2011**, *11*, 3285−3289. (b) Oh, M. H.; Yu, T.; Yu, S.-H.; Lim, B.; Ko, K.-T.; Willinger, M.-G.; Seo, D.-H.; Kim, B. H.; Cho, M. G.; Park, J.-H.; Kang, K.; Sung, Y.-E.; Pinna, N.; Hyeon, T. *Science* **2013**, *340*, 964−968.

(11) (a) Wang, D.; Li, Y. *Adv. Mater.* **2011**, *23*, 1044−1060. (b) Ferrando, R.; Jellinek, J.; Johnston, R. L. *Chem. Rev.* **2008**, *108*, 845−910. (c) Tao, A. R.; Habas, S.; Yang, P. *Small* **2008**, *4*, 310−325. (d) Kang, S. W.; Lee, Y. W.; Park, Y.; Choi, B.-S.; Hong, J. W.; Park, K.-H.; Han, S. W. *ACS Nano* **2013**, *7*, 7945−7955.

(12) (a) Bing, Y. H.; Liu, H. S.; Zhang, L.; Ghosh, D.; Zhang, J. J. *Chem. Soc. Rev.* **2010**, *39*, 2184−2202. (b) Choi, S.-I.; Choi, R. S.; Han, W.; Park, J. T. *Chem.—Eur. J.* **2011**, *17*, 12280−12284.

(13) Chen, C.; Kang, Y.; Huo, Z.; Zhu, Z.; Huang, W.; Xin, H. L.; Snyder, J. D.; Li, D.; Herron, J. A.; Mavrikakis, M.; Chi, M.; More, K. L.; Li, Y.; Markivic, N. M.; Somorjai, G. A.; Yang, P.; Stamenkovic, V. R. *Science* **2014**, *343*, 1339−1343.

(14) (a) Yin, Y.; Rioux, R. M.; Erdonmez, C. K.; Hughes, S.; Somorjai, G. A.; Alivisatos, A. P. *Science* **2004**, *304*, 711−714. (b) Macdonald, J. E.; Bar Sadan, M.; Houben, L.; Popov, I.; Banin, U. *Nat. Mater.* **2010**, *9*, 810−815. (c) Skrabalak, S. E.; Chen, J.; Sun, Y.; Lu, X.; Au, L.; Cobley, C. M.; Xia, Y. *Acc. Chem. Res.* **2008**, *41*, 1587−1595. (d) McEachran, M.; Keogh, D.; Pietrobon, B.; Cathcart, N.; Gourevich, I.; Coombs, N.; Kitaev, V. *J. Am. Chem. Soc.* **2011**, *133*, 8066−8069.

(15) (a) Wang, J. X.; Ma, C.; Choi, Y.; Su, D.; Zhu, Y.; Liu, P.; Si, R.; Vukmirovic, M. B.; Zhang, Y.; Adzic, R. R. *J. Am. Chem. Soc.* **2011**, *133*, 13551−13557. (b) Johnson, S. A.; Ollivier, P. J.; Mallouk, T. E. *Science* **1999**, *283*, 963−965. (c) Yavuz, M. S.; Cheng, Y.; Chen, J.; Cobley, C. M.; Zhang, Q.; Rycenga, M.; Xie, J.; Kim, C.; Song, K. H.; Schwartz, A. G.; Wang, L. V.; Xia, Y. *Nat. Mater.* **2009**, *8*, 935−939.

(16) Davis, R. E.; Horvath, G. L.; Tobias, C. W. *Electrochim. Acta* **1967**, *12*, 287−297.

(17) (a) Xia, B. Y.; Wu, H. B.; Wang, X.; Lou, X. W. *J. Am. Chem. Soc.* **2012**, *134*, 13934−13937. (b) Zhang, Z.; Yang, Y.; Nosheen, F.; Wang, P.; Zhang, J.; Zhuang, J.; Wang, X. *Small* **2013**, *9*, 3063−3069.

(18) Xu, Y.; Zhang, B. *Chem. Soc. Rev.* **2014**, *43*, 2439−2450.

(19) Susut, C.; Chapman, G. B.; Samjeske, G.; Osawac, M.; Tong, Y. *Phys. Chem. Chem. Phys.* **2008**, *10*, 3712−3721.

(20) Wang, D.; Yu, Y.; Xin, H. L.; Hovden, R.; Ercius, P.; Mundy, J. A.; Chen, H.; Richard, J. H.; Muller, D. A.; DiSalvo, F. J.; Abruña, H. D. *Nano Lett.* **2012**, *12*, 5230−5238.

(21) (a) Dhavale, V. M.; Unni, S. M.; Kagalwala, H. N.; Pillai, V. K.; Kurungot, S. *Chem. Commun.* **2011**, *47*, 3951−3953. (b) Unni, S. M.; Dhavale, V. M.; Pillai, V. K.; Kurungot, S. *J. Phys. Chem. C* **2009**, *114*, 14654−14661.

(22) Bard, A. J.; Faulkner, L. R. *Electrochemical Methods Fundamentals and Applications*, 2nd ed.; Wiley: New York, 2006.

(23) (a) Moulder, J. F.; Stickle, W. F.; Sobol, P. E.; Bomben, K. D. In *Handbook of X-ray Photoelectron Spectroscopy: A Reference Book of Standard Spectra for Identification and Interpretation of XPS Data*, 2nd ed.; Prairie, J. C., Minn, E., Eds.; Physical Electronics Division, Perkin-Elmer Corp.: Waltham, MA, 1992. (b) Watts, J. F.; Wolstenholme, J. *An Introduction to Surface Analysis by XPS and AES*, 2nd ed.; Wiley: New York, 2003.

DOI: 10.1021/cs501571e
ACS Catal. 2015, 5, 1445−1452